2004

Retinotopic organization in children measured with fMRI

Ian P. Conner
West Virginia University

Saloni Sharma
West Virginia University

Susan K. Lemieux
West Virginia University

Janine D. Mendola
West Virginia University

Retinotopic organization in children measured with fMRI

Ian P. Conner Department of Neurobiology & Anatomy, West Virginia University School of Medicine, Morgantown, WV, USA

Saloni Sharma Department of Radiology, West Virginia University School of Medicine, Morgantown, WV, USA

Susan K. Lemieux Departments of Radiology, Neurobiology, Anatomy, & Ophthamology, West Virginia University School of Medicine, Morgantown, WV, USA

Janine D. Mendola Departments of Radiology, Neurobiology, Anatomy, & Ophthalmology, West Virginia University School of Medicine, Morgantown, WV, USA

Many measures of visual function reach adult levels by about age 5, but some visual abilities continue to develop throughout adolescence. Little is known about the underlying functional anatomy of visual cortex in human infants or children. We used fMRI to measure the retinotopic organization of visual cortex in 15 children aged 7–12 years. Overall, we obtained adult-like patterns for most children tested. We found that significant head motion accounted for poor quality maps in a few tested children who were excluded from further analysis. When the maps from 10 children were compared with those obtained from 10 adults, the magnitude of retinotopic signals in visual areas V1, V2, V3, V3A, VP, and V4v was essentially the same between children and adults. Furthermore, one measure of intra-area organization, the cortical magnification function, did not significantly differ between adults and children for V1 or V2. However, quantitative analysis of visual area size revealed some significant differences beyond V1. Adults had larger extrastriate areas (V2, V3, VP, and V4v), when measured absolutely or as a proportion of the entire cortical sheet. We found that the extent and laterality of retinotopic signals beyond these classically defined areas, in parietal and lateral occipital cortex, showed some differences between adults and children. These data serve as a useful reference for studies of higher cognitive function in pediatric populations and for studies of children with vision disorders, such as amblyopia.

Keywords: vision, development, pediatric, neuroimaging, neurons, visual areas, hemispheric laterality

1. Introduction

Psychophysical measurements in humans have established that the visual system depends extensively on postnatal experience to guide developmental mechanisms and eventually reach a mature state. Although perhaps the most dramatic improvements in performance occur in the first year of life, some abilities require many years of visual experience to achieve the adult-like state. For example, some measures of basic vision, such as grating acuity, do not reach adult values before age 6. Temporal contrast sensitivity at high frequencies (20 and 30 Hz) and critical flicker fusion frequency are adult-like at age 4, although contrast sensitivity for lower temporal frequencies and static gratings matures between ages 4 and 7 (Ellemberg, Lewis, Liu, & Maurer, 1999). Even later maturation of several visual functions that require global integration across distance in the visual field has been recently documented. For example, texture segregation does not reach adult levels until between ages 14 and 18 (Sireteanu, 2000). Contour integration has been shown to have a protracted development when tested with oriented Gabor element textures, and with the Ebbinghaus illusion (Kovacs, Kozma, Feher, & Benedek, 1999; Kovacs, 2000). Finally, Vernier hyperacuity undergoes a steep improvement during childhood until adult levels are reached at age 14 (Skoczenski & Norcia, 2002).

Much less is known about the physiological maturation of the visual system during childhood. One of the few available techniques is noninvasive electrical recording from the scalp, and such data indicate ongoing neural development through childhood. For example, the checkerboard onset evoked potential does not obtain its adult form before puberty (Ossenblok De Munck, Wieringa, Reits, & Spekreijse, 1994). Evoked potentials and visual performance measures sometimes show nice parallels, but not always (Regan & Spekreijse, 1986; Tyschen, 1992). Interestingly, some evidence suggests that the responses of visual neurons are often more mature than behavioral measures would predict (e.g., Kiorpes & Movshon, 2003), although the reasons for this discrepancy are still unclear.

The advent of noninvasive functional neuroimaging (fMRI) provides new opportunities to improve understanding of the functional neuroanatomy of humans in health

doi:10.1167/4.6.10 Received October 13, 2003; published June 18, 2004 ISSN 1534-7362 © 2004 ARVO

and in disease. Although the source of the measured signal is hemodynamic, not neural, it is coupled to neural activity (e.g., Logothetis, Pauls, Augath, Trinath, & Oeltermann, 2001) with an impressive spatial (2-4 mm) and temporal (1-2 s) resolution. These techniques can be applied to pediatric populations, and have been done so increasingly (e.g., Casey et al., 1995; Kwon et al., 2002; Temple et al., 2003; Turkeltaub, Gareau, Flowers, Zeffiro, & Eden, 2003). Most efforts have focused on cognitive functions, such as reading ability and memory. The majority of such studies provide stimuli through the visual modality. Therefore, it is important to understand the state of maturity of early visual areas in this age range for better interpretation of cognitive studies, as well as to directly investigate human visual system development.

Retinotopic organization of human visual cortex has been mapped using functional magnetic resonance imaging (fMRI) in adults. Multiple visual areas have been shown to exist, each with its own representation of visual space (Sereno et al., 1995, DeYoe et al., 1996; Engel, Glover, & Wandell, 1997). This type of mapping of visual cortex is important for several reasons. 1. The technique allows for rapid delineation of a large expanse of visual cortex. 2. The boundaries of several visual areas can be defined by the representations of the horizontal and vertical meridians of visual space. Such objective boundaries guide the creation of regions of interest that can be applied in a statistically independent way to the results of other experiments. 3. By mapping a fundamental and continuously changing variable across the cortical sheet, significant information can be acquired about *intra*-areal function.

These powerful noninvasive methods for mapping retinotopic function have not previously been extended to children. Here we show that visually normal children have essentially achieved an adult-like pattern of many retinotopic visual areas mapped with functional magnetic resonance techniques, at least by age 9. However, quantitative differences were detected between the adult and child groups in the size of visual areas. To extend our results beyond these well-known areas, we also employed new cortical-surface-based methods for achieving inter-subject averaging. Different patterns of activation in parietal and lateral occipital cortices were observed. These data can serve as an important baseline from which to compare the retinotopic maps of normal children to those with visual disorders.

2. Methods

2.1 Subjects

We studied 10 adults aged 21 to 30 years (6 male, 4 female) and 15 children aged 7 to 12 years (7 male, 8 female). Seven child subjects were less than 10 years and 8 were greater than or equal to 10 years. After excluding from analysis subjects exhibiting significant head motion, 10 subjects remained, and their ages were 9, 9, 10, 10, 10, 11, 12, 12, 12, and 12 years. With regard to the handedness of our subjects, 9/10 adults were right-handed, and 8/10 children were right-handed.

Our subjects were recruited from the local community surrounding West Virginia University (WVU). Informed consent was obtained from all subjects in a project approved by the WVU Institutional Review Board for the Protection of Human Subjects (protocol #14788).

2.2 Cortical surface reconstruction

Surface reconstructions of each subject's cerebral cortex were generated from high-resolution anatomical images obtained in a General Electric 1.5 Tesla MR scan session separate from the retinotopic mapping experiments. Previously validated techniques (Dale, Fischl, & Sereno, 1999; Fischl, Sereno, & Dale, 1999a) were employed. Briefly, brain reconstruction was begun by collecting whole-head 3D fast spoiled grass gradient echo (FSPGR) scans, optimized for contrast between gray and white matter, for each subject. Specific parameters were fast IR prep (prep time = 300 ms), TE = 1.9 ms, flip angle = 20 deg, FOV = 24 cm, axial slices, 256 × 256 matrix, resolution 0.94 × 0.94 × 1.2 mm.

The surface reconstructions were created using the FreeSurfer software package available at http://www.nmr.mgh.harvard.edu/freesurfer. Voxels containing white matter in an intensity-normalized volume were labeled using an anisotropic planar filter. A region-growing algorithm was then used to ensure that each cortical hemisphere was represented by a single connected component with no interior holes. The surfaces of these components were tessellated (~150,000 vertices), refined against the MRI data using a deformable template technique, and manually inspected for topological defects (i.e., departures from spherical topology). Automated techniques for optimizing topological correctness while maintaining geometrical accuracy were employed (Fischl, Liu, & Dale, 2001).

In a separate step, the cortical surface was computed by expanding the gray/white surface by 3 mm and refining it against the FSPGR MR images. The sampled functional signal included most of cortical gray matter, but it was centered just above the gray/white boundary to avoid the pial surface where macrovascular fMRI artifacts are greatest, and to ensure that functional signals were assigned to the correct sulcal bank. The surface reconstruction of each subject's brain was "inflated" by an iterative algorithm that reduced local curvature while approximately preserving local areas and angles by minimizing metric distortion.

Once a cortical surface is reconstructed, it becomes possible to calculate the surface area of the entire cortical sheet, or of smaller cortical areas defined as regions of interest (ROI). Although the ROIs can be drawn (i.e., defined) on the flattened surface, the ROIs are mapped back to the folded cortical surface when measurements are made, avoiding the areal distortion created by inflation and flattening. Measures of surface area are made at the

gray/white boundary, as this best represents the location of recorded functional signals. We compute the area associated with the polygonal surface model, which is very densely sampled. The area of each triangular vertex is approximately 0.5 mm^2. The area of an ROI is the sum of the area of *n* triangles. Due to the inherent difficulty of segmentation of white from gray matter, segmentation is a potential source of error in the reconstructions. However, the accuracy of the programs has been validated (e.g., by test-retest comparisons) (Dale et al., 1999) and the accurate estimates of cortical thickness (Fischl & Dale, 2000; Rosas et al., 2002). Furthermore, each reconstruction is manually inspected for errors.

2.3 Functional magnetic resonance imaging

Subjects were scanned in a GE 1.5 Tesla MR scanner using techniques described previously (Mendola, Dale, Fischl, Liu, & Tootell, 1999). After a sagittal localizing scan was obtained, a T1-weighted inversion recovery sequence (TR = 400 ms) was used to acquire 20 interleaved 4-mm slices with 0.86 × 0.86 mm in-plane resolution, oriented perpendicular to the calcarine sulcus. These anatomical scans were later used to register the functional scans to the FSPGR slices that were used to define the cortical surface.

The next step was to acquire multiple functional scans using the same slice prescription selected in the anatomical scans, but with 3.44 × 3.44 mm in-plane resolution. Functional signals reflecting neural activity via local oxygen consumption and blood flow were acquired (after Kwong et al., 1992; Ogawa et al., 1992) using a spiral gradient echo sequence (TE = 40 ms, TR = 4000 ms, flip angle = 65 deg, FOV = 22 cm, matrix 64 × 64 (Glover, 1999).

For the adults, functional scans had a duration of 8 min and 32 s, and 128 time points were collected from each slice in all scans. Four scans of this type were administered in one session, two scans for eccentricity and two scans for polar angle. For the children, functional scans had a duration of 4 min and 16 s, and 64 time points were collected from each slice in all scans. Six scans of this type were administered in one session, three scans for eccentricity and three scans for polar angle. The entire scanning procedure typically lasted about 2 hr.

Head movement (within and between scans) was minimized by the use of one of two methods. Most subjects used a bite bar, in which subjects stabilized their jaw in a rigid, deep individual dental impression, mounted in an adjustable frame. For children who were not comfortable using a bite bar, we used a rigid chin cup that greatly restricted movements in all planes. Although we did not monitor eye movements, the good quality of our retinotopic maps indicates adequate fixation during the functional scans. Our use of radial motion and symmetric stimuli also helps to minimize translational eye position drifts.

2.4 Visual stimuli

During the fMRI experiments, the visual stimuli were generated by a Silicon Graphics O2 computer with an output resolution of 640 x 480 pixels. The video output was converted to a 60-Hz interlaced composite S-VHS signal, which served as input to an Epson Powerlite 500c LCD projector. The projector's image passed into the bore of the magnet, and appeared on a paper rear-projection screen in front of the subject. The subjects viewed the screen by looking straight up at a mirror placed at an approximately 45-deg angle to both the screen and the subject's line of sight. The stimuli subtended an area of about 25-deg horizontal by 15-deg vertical.

The cortical representation of retinotopic visual space was mapped with a phase-encoded design in which the cardinal axes of space (eccentricity and polar angle) were mapped separately (Engel et al., 1994; DeYoe et al., 1996; Engel et al., 1997). The stimuli consisted of high-contrast, chromatic, flickering checkerboard patterns of two specific types. The "rotating wedge" stimulus would sweep through polar angles much like a hand on a clock, and the "expanding ring" stimulus mapped eccentricity by starting from the center of the visual field and expanding outward (Figure 1). Eccentricity stimuli traversed space with a logarithmic transformation, as has been used previously (Sereno et al., 1995; Tootell et al., 1997). Both stimuli attempted to compensate for the cortical magnification factor by increasing in size as they approach the periphery. These phase-encoded stimuli always used a cycle length of 64 s, which corresponds to 8 cycles per scan for adults and 4 cycles per scan for children. Adults were shown 16 cycles of each stimulus type, whereas children were shown 12 cycles. The lower number of cycles was used for the children due to concerns about their stamina for accurate fixation and minimal head motion. However, the number of cycles was equated between groups at the subsequent analysis stage by excluding a portion of the adult data.

A central fixation mark was present at all times for all stimuli. Subjects were clearly instructed to maintain fixation on this mark at all times during an fMRI scan. Subjects were also instructed to perform a task monitoring the appearance of the fixation point to aid fixation stability. The fixation point briefly changed color from white to red with an inter-trial interval that randomly ranged from 4-32 s (in 4-s multiples) during the course of an fMRI scan, and the subjects pressed a key upon detecting such a change. The children were able to perform this task at a very accurate level (mean = 98% correct).

2.5 Statistical analysis

2.5.1 Individual subject analysis

The functional analysis was completed using the FS-FAST software tools freely available at ftp://ftp.nmr.mgh.harvard.edu/pub/flat/fmri-analysis. A brief description of the processing steps follows. For each subject, raw

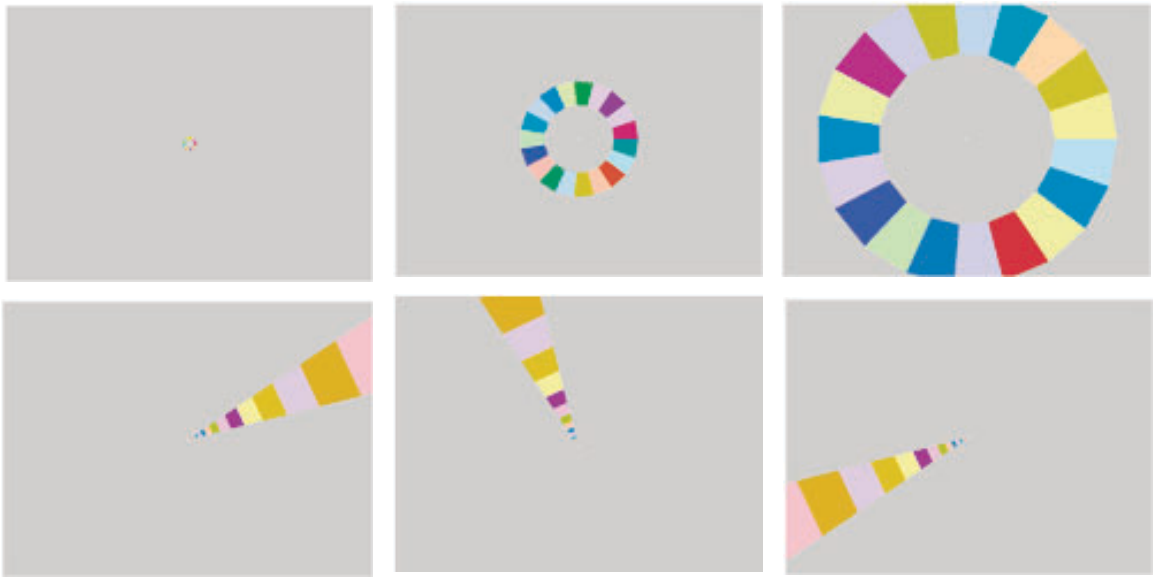

Figure 1. Depiction of dynamic eccentricity and polar angle stimuli. Top. The eccentricity stimulus was an annular ring that slowly expanded in size. Three isolated example frames are shown. Bottom. The polar angle stimulus was a wedge that rotated around the fixation point.

MR images were first motion-corrected using an iterated, linearized, weighted-least-squares method through the FSFAST implementation of the AFNI 3dvolreg algorithm (Cox & Jesmanowicz, 1999), and then intensity-normalized using the average in-brain voxel intensity. The residual, uncorrectable head motion was measured as the root mean square (RMS) difference between motion-corrected output and a target volume defined from the middle time point of each scan. This value was computed for each subject, and values exceeding a RMS of 60, which corresponded to the grossly observed image artifacts, were used as a criterion for exclusion of some of the children (5/15) from further processing. For the remaining 10 subjects, the average corrected motion in all three planes was quantified as the vector magnitude of translational motion.

After the preprocessing steps, a fast Fourier analysis was conducted on the time series of each voxel to statistically correlate retinotopic stimulus location with visual cortical anatomy. To equate the children and adults for data analysis, only the first 12 cycles were analyzed for the adults. This analysis rejects low frequencies due to subject head motion or baseline drift and extracts functional signals in the form of magnitude and phase relative to the stimulus cycle frequency (8 or 4 cycles per scan; period = 64 s). Signal magnitude reflects the degree of retinotopic specificity, which can be low due to either a lack of visually induced response or to an equal response to all retinotopic locations. The phase component of the signal was used to code retinotopic location. Activation significance (F) values were computed for each voxel by using a comparison between the Fourier domain amplitude at the stimulation frequency and the average amplitude at other (nonharmonic) frequencies. For these types of calculations, the phase/magnitude data are converted from polar coordinates to the equivalent data in rectilinear coordinates (i.e., complex numbers with real and imaginary components). The F statistic accommodates this multivariate analysis. The F statistic is computed as the sum of the squared real and imaginary signal components divided by the noise variance. Finally, a registration procedure within Freesurfer was used to align (in all 3 planes) the T1 contrast anatomical images collected in each functional session with the cortical surface model. The same registration matrix was then applied to the functional images to view the results on the cortical surface.

The data from the paired eccentricity and polar angle scans were combined to yield field sign maps. The field sign maps the polarity of the visual field representation as either similar to the actual visual field geometry or mirror symmetrical to it. The field sign for each cortical area was objectively calculated from the vector product of the constituent phase-encoded maps of polar angle and eccentricity as in Sereno et al. (1995). Visual area naming conventions are as described in Tootell et al. (1997), and are consistent with previous studies. The superior portions of V1, V2, and V3 contain representations of the contralateral lower visual field, whereas the inferior portions of V1, V2, VP, and V4v represent the contralateral upper visual field. V3A represents both the lower and upper contralateral field. Areas V1, V2, VP, V3, V3A, and V4v are classical retinotopic areas that have been described previously. We did not attempt to explicitly identify retinotopic areas anterior to these areas. There are additional retinotopic areas, including V7 and V8, whose cruder retinotopy has been demonstrated only with high-field scanning (Hadjikhani, Liu, Dale, Cavanagh, & Tootell, 1998; Tootell et al., 1998a; Wade, Brewer, Rieger,& Wandell, 2002). Also, there is still debate regarding the appropriate definition of visual areas in this region. This fringe retinotopy region has also been

shown to be activated by both left and right visual fields (Tootell, Mendola, Hadjikhani, Liu, & Dale, 1998b). Thus, the evidence suggests that areas V7 and V8 lie near the end of a continuum of decreasing retinotopy and increasing receptive field sizes.

2.5.2 Region of interest analysis

To generate ROIs specific to a given visual area, patches of flattened cortex that corresponded to each retinotopic area were defined based on the retinotopic field sign map for each subject (Mendola et al., 1999). These objectively defined borders were available for visual areas V1, V2 (superior and inferior), V3, VP, V3A, and V4v. The eccentricity range of these ROIs was approximately 1-15°. Specifically, the vertical eccentricity was 7.5° and the horizontal eccentricity was 12.5°, making the maximum (diagonal) eccentricity 15°. The outer extent of the ROI was based on the actual activation present. Because the resolution of these maps is typically too low to measure the extremely high cortical magnification factor in the central foveal representation, the ROIs did not include the entire foveal representation. The minimum eccentricity value varied slightly from subject to subject, but was between 1-2 deg for most (see Figure 5). For each subject, the Freesurfer software program was used to draw the outline of each visual area for each hemisphere. In this way, we defined the boundaries of six visual areas for the 10 adults and 10 children with interpretable field sign maps. For visual area V2, an ROI was drawn for the superior/dorsal branch and another for the inferior/ventral branch (see Figure 2), although the results for these branches were combined in subsequent analysis. For all RO1s except V1, the flattened cortex was used for visualization. For V1, the inflated cortex was used for visualization so that the split along V1 in the flattened view did not interfere with definition. Regardless of the view chosen for visualization, all ROIs exist in native (folded) coordinates when measurements are made.

2.5.3 Cortical magnification factor analysis

To further compare the internal organization of the V1 and V2 retinotopic map in children and adults, we computed the cortical magnification function as has been done previously by others for adult subjects (Sereno et al., 1995; Engle et al., 1997; Duncan & Bonton, 2003). This first required definition of an approximately iso-polar ROI along the representation of the horizontal meridian within V1 for every subject. This was done by applying a filter to the V1 ROI to accept voxels with polar angle phase values at the horizontal meridian (90 deg) ± 15 deg. We then determined the eccentricity phase values of all voxels in this ROI. These voxels were sorted according to distance from a reference point at the occipital pole defined in every subject. The distance was computed as the arc distance along the inflated cortical surface in spherical space, allowing us to express distance along the cortical sheet, regardless of cortical folding pattern. The distance of each voxel was then plotted against its eccentricity phase value (or the equivalent degrees of visual angle). Finally, this curve was fit with an exponential function that best fit the least square data. Specifically,

$$y = y_0 e^{kx},$$

where x is the cortical distance and y is the eccentricity. The process for V2 was equivalent, except that the 30-deg filter was centered on oblique polar angles (135 deg for V2v and 45 deg for V2d), so as to fall along the center of those areas. One adult subject and one child subject, with poor quality polar angle maps, did not satisfy our criteria of least squares R^2 fit greater than 0.5, and were excluded from this analysis.

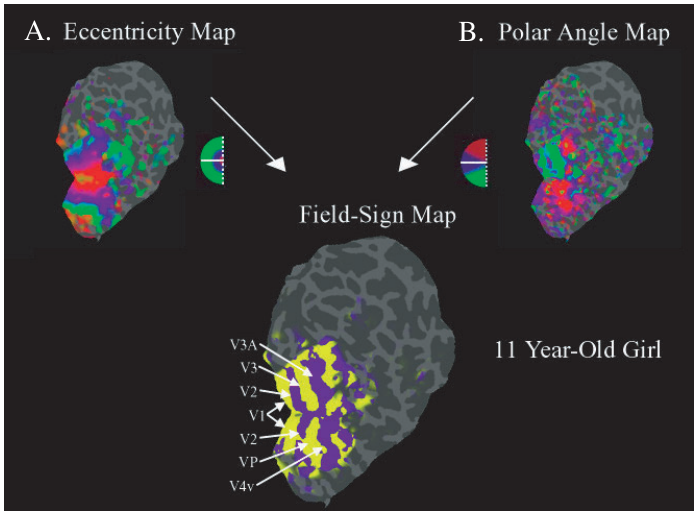

Figure 2. Retinotopic mapping results from one child. A. Eccentricity representation is shown on a flattened representation of the right occipital pole. Light and dark grays indicate the unfolded gyri and sulci, respectively. Red, green, and blue indicate the central 1.5-deg, 1.5-5-deg, and 5-15-deg eccentricity. The adjacent semicircular logo depicts this color scheme in the corresponding left visual field. B. Polar angle representation is shown in the same subject. As indicated in the adjacent logo, red and green indicate the upper and lower vertical meridians, and blue indicates the horizontal meridians. C. Data sets in A and B are combined to yield the field sign map that indicates the boundaries of multiple visual areas. Yellow indicates areas with quarter or hemi-field representation; blue areas have the opposite field sign (i.e., a mirror-reversed map).

2.5.4 Across-subject analysis

Directly averaging fMRI data across subjects is an inherently difficult task, due to the differences in the size, shape, and even functional organization of subjects' individual brains. Using common spaces, such as the traditional neurosurgical space of Talairach and Tournoux (1988) or even more modern versions such as the space defined by 152 adult subjects at the Montreal Neurological Institute (Evans et al., 1993), introduces a large amount of spatial blurring into the data set. Typical variability between

presumably homologous points in subjects is of the order of 1 cm in Talairach space. Given that individual visual areas have a (flattened) width of about 1 cm, such averaging procedures seriously degrade the quality of retinotopic maps. Nonetheless, across-subject averaging remains a desirable goal. Specifically, to compare the retinotopic maps obtained beyond the 6 defined visual areas in parietal and temporal cortex, we need a strategy that does not require ROIs.

Thus, to compare the adult and child groups, we used a new technique for across-subject analysis, adapted to the folding pattern of each subject, that is significantly more accurate (Fischl, Sereno, Tootell, & Dale, 1999b). Each adult's inflated cortical surface was first registered to a standardized average inflated unit-sphere based on alignment of gyral and sulcal patterns using techniques described elsewhere (Fischl et al., 1999b). To combine functional data across individuals for a group comparison, *F*-value data sets were then re-sampled into spherical space and subsequently averaged across subjects using a fixed-effects model (i.e., *F* ratio numerator is summed real plus imaginary components squared, and denominator is the summed noise variance divided by number of subjects). Extension of these methods to random effects is desirable, but will require accounting for multiple comparisons on the surface, and clustering approaches may not be appropriate for retinotopic data. Finally, the average *F*-value map was painted (via the spherical transformation) onto the inflated surface of one adult. Separate maps were created for the eccentricity and polar angle stimulus in each hemisphere. The entire analysis was subsequently repeated for the group of children.

It should be noted that the standardized spherical template currently available in Freesurfer was created with adult brains. Therefore, the children's brains require somewhat more distortion than the adult's when placed into spherical space. To document this, the Jacobian determinant of each vertex can be computed to indicate how much the transformation expands or shrinks each vertex in the brain (expansion results in values greater than 1, whereas contraction produces values less than 1). For the entire right hemisphere, the mean adult variance from 1 was 1.5, whereas the child variance was 2.1, whereas left hemisphere values were 1.4 and 2.1. The comparison of variances across groups with a *t* test approached significance ($p = .06$ and $p = .05$, respectively).

3. Results

3.1 Individual phase-encoded maps

Maps of eccentricity and of polar angle were obtained as has been reported previously for adult subjects (Sereno et al., 1995). Eccentricity maps showed the well-known organization, with central vision represented at the pole and peripheral vision more anteriorly. Polar angle maps were obtained with vertical meridian representation separating V1 and V2, and horizontal meridian separating V2 from V3 and VP. V3 and VP were separated from V3A and V4v by lower and upper vertical meridian, respectively. Similar maps were obtained from the children (Figure 2A and 2B).

To better localize the boundaries between areas, we used the eccentricity and polar angle data to compute a field sign map (Sereno et al., 1995). All adult subjects produced maps of sufficient quality to identify the six retinotopic areas described for humans (V1, V2, V3, VP, V3A, and V4v). We obtained interpretable maps in 10 of 15 children, and these maps were qualitatively similar to those seen in adult subjects. An example is shown of one 11-year-old subject (see Figure 2C).

Observation during the experiments, subjective reports from the children, and head motion artifacts indicated that head motion likely contributed to the poor quality of maps in the other five subjects. Four of these subjects were among the youngest subjects, 7-9 years old. These subjects were excluded from further analysis.

3.2 Head motion

To quantify the head motion in each of the experimental scans, we used the motion-correction algorithm in AFNI. For each subject we extracted the average motion in all three directions as the vector magnitude of translational motion. This value ranged from 0.2-0.5 mm for adults and 0.3-2.0 mm for children (Figure 3). Pearson Product correlations were performed to look for any consistent relation between age and corrected head motion, especially in the young group. We did not find a significant correlation in the child group ($R^2 = 0.07$) or the adult group ($R^2 = 0.34$).

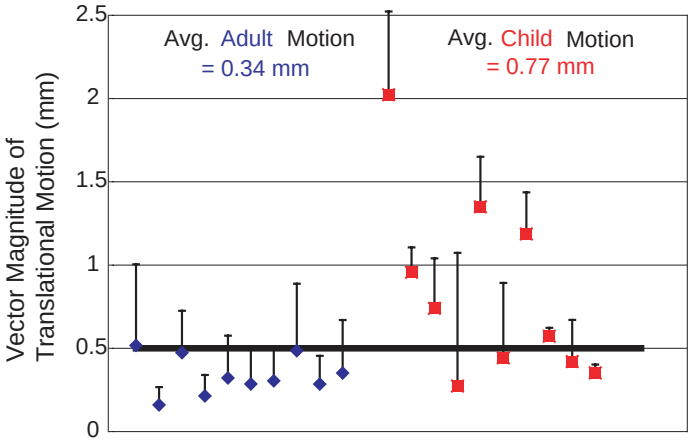

Figure 3. Comparison of average head motion during the fMRI scans for adults and children. Each data point represents the vector magnitude of translational head motion detected by the motion-correction algorithm. Adults are indicated with blue diamonds, children with red squares. As a population, children produced more movement, but some children were indistinguishable from adults. The thick horizontal black line serves as a reference mark.

3.3 Region of interest analysis for across group comparisons

Thus far, *qualitative* inspection of the retinotopic maps from representative children and adults did not suggest consistent differences between groups. However, it is important to be able to *quantify* measures from individual visual areas that can be averaged across subjects to address any systematic group differences. For the 10 adults and 10 children with interpretable field sign maps, regions of interest were created for the six visual areas (V1, V2, V3, V3A, VP, and V4v). A seventh ROI entitled "All" was defined to include all six visual areas. These ROIs were used to separately extract from our data the average fMRI signal Fourier magnitude of all voxels located in each of the six visual areas. We also directly calculated the surface area of visual area ROIs as described in Section 2.2.

3.3.1 Measures of signal magnitude

The average Fourier magnitude was calculated for all voxels in a given visual area, for the left and the right hemispheres separately. The results are listed in Tables 1 and 2.

Direct comparison between evoked fMRI signal in each area for adults and children was performed with *t* tests. For the polar angle stimulus, only the right VP was significantly different, having a larger value in adults. Next section we consider this difference in relation to the size of the visual areas.

Pearson Product correlations were also performed to look for any developmental relation between age and Fourier magnitude, as well as between corrected head motion and signal magnitude, especially in the young group. There were no significant correlations between magnitude and head motion for either group. There were several visual areas that showed a significant correlation between magnitude and age within the child group. However, the magnitude was negatively correlated with age, and may be due, in part, to the unusual coincidence that four of our youngest children were scanned on the same day. Also, the areas showing this correlation were not consistent between hemispheres. No correlations with age were significant for the adult group.

3.3.2 Measures of visual area size

For each subject in both groups, the size of the six visual areas was analyzed in terms of absolute surface area in mm^2, and as a relative proportion of the total cortical sheet. The adult group and the child group were then directly compared. The results are listed in Tables 3 and 4.

Visual Area	Child LH polar	Adult LH polar	Sig. *p* LH polar	Child LH eccen	Adult LH eccen	Sig. *p* LH eccen
V1	3.1	2.6	-	7.6	5.4	-
V2	3.7	3.3	-	9.5	6.7	-
V3	5.7	4.7	-	12.4	9.3	-
V3A	5.3	4.1	-	9.3	7.2	-
VP	4.0	3.9	-	9.8	6.4	-
V4v	3.9	4.1	-	5.7	5.6	-
All	25.7	22.7	-	54.3	40.6	-

Table 1. Left hemisphere differences between children and adults for polar angle and eccentricity Fourier magnitude across visual areas.

Visual Area	Child RH polar	Adult RH polar	Sig. *p* RH polar	Child RH eccen	Adult RH eccen	Sig. *p* RH eccen
V1	2.0	3.0	-	5.8	4.9	-
V2	3.1	4.0	-	8.4	7.1	-
V3	6.3	5.1	-	13.0	7.6	-
V3A	4.5	3.1	-	7.8	6.6	-
VP	3.2	5.2	0.007	8.6	8.3	-
V4v	4.9	4.1	-	8.9	5.8	-
All	24.0	24.5	-	52.4	40.3	-

Table 2. Right hemisphere differences between children and adults for polar angle and eccentricity Fourier magnitude across visual areas.

Visual Area	Child LH mm^2	Adult LH mm^2	Sig. *p* LH mm^2	Child LH %	Adult LH %	Sig. *p* LH %
V1	1102	1182	-	1.3	1.4	-
V2	851	1194	0.02	1.0	1.4	0.02
V3	417	580	0.04	0.5	0.7	0.05
V3A	513	678	-	0.6	0.8	-
VP	496	678	-	0.6	0.8	-
V4v	484	738	0.01	0.6	0.9	0.02
All	3865	5049	0.02	4.7	5.5	0.03

Table 3. Left hemisphere differences between children and adults for visual area size.

Visual Area	Child RH mm^2	Adult RH mm^2	Sig. *p* RH mm^2	Child RH %	Adult RH %	Sig. *p* RH %
V1	1219	1155	-	1.5	1.4	-
V2	866	1161	0.02	1.1	1.4	0.04
V3	381	502	0.04	0.5	0.6	0.07
V3A	549	540	-	0.7	0.6	-
VP	462	667	0.003	0.6	0.8	0.02
V4v	597	648	-	0.7	0.8	-
All	4073	4673	0.07	5.1	5.6	-

Table 4. Right hemisphere differences between children and adults for visual area size.

The size of visual areas in both adults and children covers a range of about 400-700 mm^2, except for V1 and V2, which ranged from 800-1200 mm^2. The results indicated some small but significant differences between the adults and children. Adults showed a slightly larger extent of visual areas V2, V3, and V4v in the left hemisphere. In the right hemisphere, visual areas V2, V3, and VP were significantly larger in adults. In contrast, there was no difference in the extent of V1 between groups.

One concern with the use of an absolute measure of visual area ROI size is that children's brains might be globally smaller than adult's. Hence, we compared cortical surface area for the entire neocortical reconstruction of each hemisphere between children and adults. The left and right hemisphere reconstructions yielded a mean measure of 81,734 and 81,128 mm^2 for the children, and 87,009 and 86,011 mm^2 for adults. The adult's brains were larger than the children's brains, but the effect was not significant (p = 0.12 for left hemisphere; p = 0.13 for right hemisphere). Nevertheless, given the obvious developmental trend, a measure of ROI size relative to the total neocortical sheet may be a valuable measure (Tables 3 and 4). Overall, individual visual areas range from 0.5-1.5% of the cortical sheet, and all six visual areas combined occupy about 5% of the neocortex in one hemisphere. When the adults and children were compared, the results were highly consistent with the comparisons of absolute size in that similar extrastriate areas proved to be slightly larger in adults. The total proportional size of the visual areas of both hemispheres in children and adults is shown graphically (Figure 4).

Pearson Product correlations were performed to look for any consistent developmental relation between age and surface area, especially in the young group. However, we found no significant correlations for the child or the adult group.

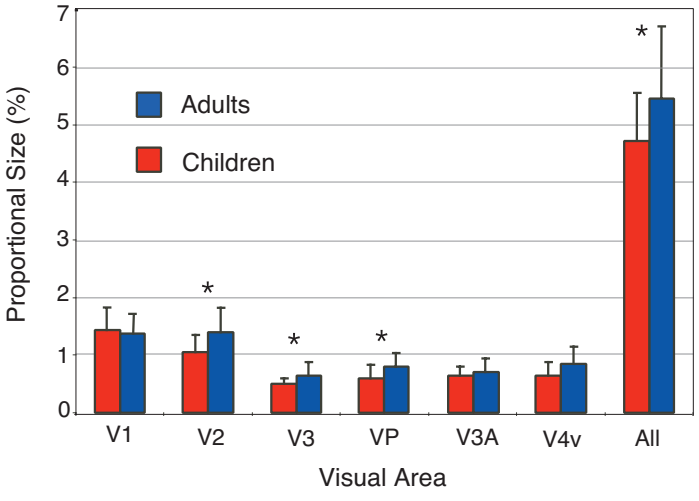

Figure 4. Comparison of size of visual areas in children and adults. The total combined area (as a percentage of the entire cortical sheet) of homologous visual areas in both hemispheres is plotted. A significant difference between groups is indicated with an asterisk.

It is interesting to consider the fact that the mean level of Fourier magnitude did not differ between children and adults, yet we observed a correlation between Fourier magnitude and children's age. In contrast, mean areal size did differ between children and adults, yet no correlation was found between size and age. This suggests that the Fourier magnitude measure was more variable than areal size, and this is indeed the case. To document this efficiently, we calculated the coefficient of variance (CV) as the *SD* divided by the mean. Fourier magnitude measures for children's visual areas had a CV in the range of 50-55%; adults produced values ranging from 35-45%. Measures of areal size (absolute and normalized) had a CV in the range of 15-30% for both children and adults.

It is well known in the neuroimaging field that magnitude of fMRI signals cannot typically be separated from the extent of activation. However, in the case of phase-encoded retinotopy, the situation is different. Signal magnitude is not directly used to determine the size of the visual areas, although a minimal magnitude is required to carry the phase-encoded signals. The preceding paragraph certainly documents that these two variables showed different patterns in our results. For a few visual areas, we did observe a significant correlation between Fourier magnitude and area size, but these did not dominate the data set and showed no clear consistency. Specifically, for children, normalized area was correlated with magnitude for left V4v and right V2 for eccentricity, and right All for polar angle. For adults, normalized area was correlated with magnitude for left VP for eccentricity, and left V4v for polar angle.

3.4 Cortical magnification function for across-group comparisons

In addition to measures of Fourier magnitude, our methods provide information about the phase of the MRI signal for each voxel within a visual area. A smooth progression of phase values is produced by the eccentricity and polar angle stimuli (the retinotopic map). An important feature of this map is the amount of cortex devoted to representing a unit of visual space, and this can be plotted as a cortical magnification function. We computed the cortical magnification function for areas V1 and V2 in children and adults. For each subject, we plotted stimulus eccentricity versus cortical distance from the occipital pole along the horizontal meridian in V1.

The curves from each subject were well fit by exponential functions (R^2 > 0.5). Moreover, the average adult and children curves were fit with R^2 values of 0.94 and 0.96, respectively (Figure 5). The mean fitted exponent was 0.74 for the adults and 0.71 for the children. The two subject groups did not have a different distribution of exponential values. This was true when the fit was done after placing

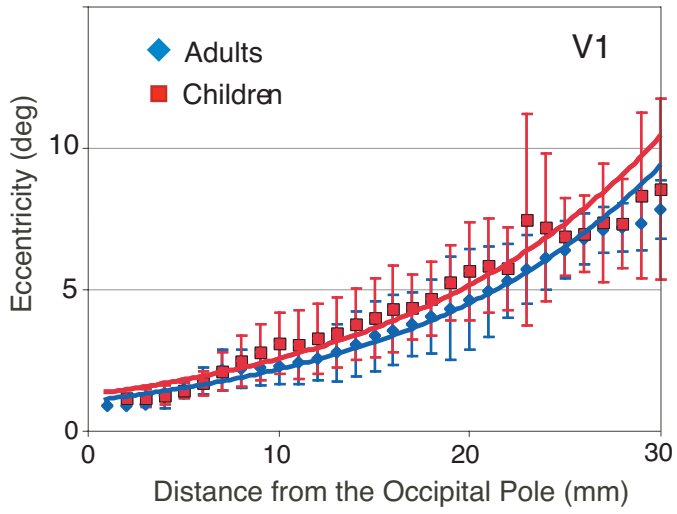

Figure 5. Comparison of cortical magnification functions in area V1 for children and adults. Eccentricity is plotted against cortical distance from the occipital pole along the horizontal meridian.

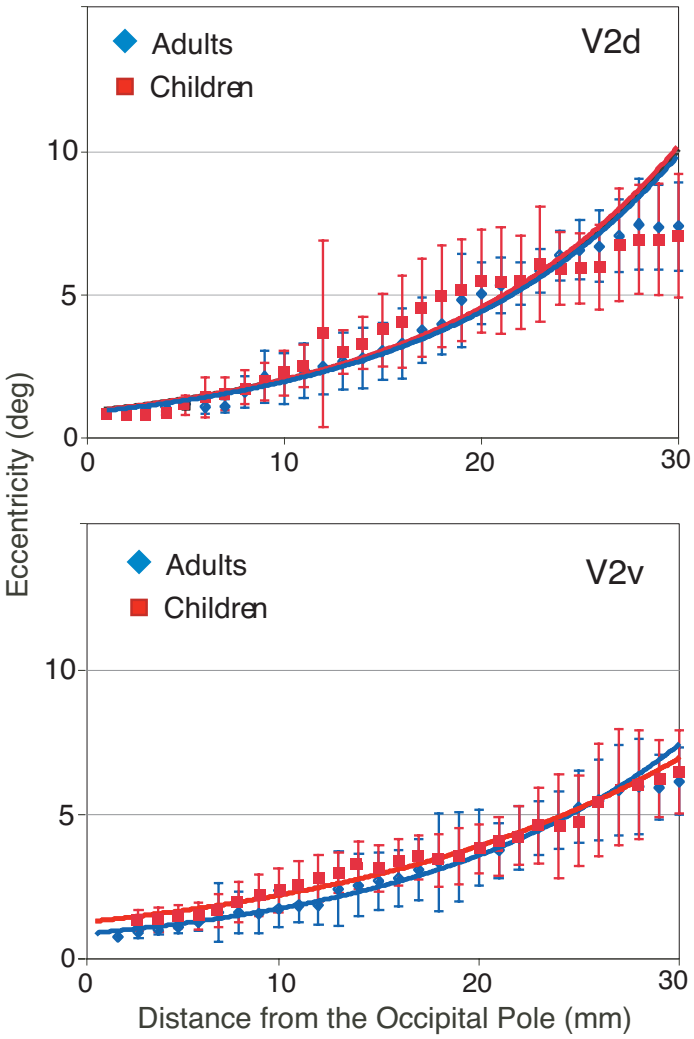

Figure 6. Comparison of cortical magnification functions in areas V2v and V2d for children and adults. Eccentricity is plotted against cortical distance from the occipital pole.

data in 1-deg bins to make Figure 5 (p = .66) and in the case of the non-binned data (p = .96). Thus, our data indicate no difference in the precise retinotopic mapping function, although it can be seen that the variance of the child group was somewhat greater.

For V2, we measured the cortical magnification function for both the ventral and dorsal branch, V2v and V2d (Figure 6). The results were similar to those for V1. Specifically, for V2v we obtained R^2 values of 0.98 and 0.97 for adults and children. The mean fitted exponential value is 0.073 for the adults and 0.057 for the children. For V2d, R^2 values are 0.96 and 0.92 for adults and children. The mean fitted exponential value is 0.081 for the adults and 0.080 for the children. The two subject groups do not have a different distribution of exponential values for V2v (p = .66) or V2d (p = .99). With regard to any differences between the exponential function for V2v and V2d, there is a significant difference for the children (p = .01) with V2d showing a steeper slope than V2v. The same trend is observed in adults.

3.5 Cortical surface averaging for across-group comparisons

The parietal, lateral occipital, and temporal cortical regions are not thought to contain precise retinotopic maps, but cruder retinotopic biases may, in fact, exist (e.g., Malach, Levy, & Hasson, 2002; Hasson, Levy, Behrmann, Hendler, & Malach, 2002). To compare phase-encoded retinotopic signals in these regions, we could not use the ROI strategy because the field sign maps do not extend into these cortices, and thus do not provide a method for identifying visual area boundaries. Using anatomically defined ROIs to directly compare children and adults was rejected due to uncertainty regarding homologous points in the cortex of these two groups. The two groups could nevertheless be compared by creating maps that show the average activation pattern for all children and for all adults.

Specifically, we used a new technique for performing across-subject averaging (Fischl et al., 1999b). This new solution is based on a spherical surface template, and provides significantly improved accuracy over volume-template techniques. This method uses the cortical surface reconstructions that we made for every subject, is based on localizing position relative to the 2D cortical sheet, and is adapted to the folding pattern of each individual subject.

We thus made across-subject averages of the statistical measure of Fourier magnitude based on the F statistic. Average F-statistic maps were produced for the adult group and the children's group. The results for the eccentricity stimulus indicate a larger extent of signal in the adult subjects in parietal cortex (Figure 7). Inspection of the individual data revealed that this was a consistent trend in the groups, for both hemispheres. Seven out of 10 adults showed some activation in the middle and/or anterior extent of the intraparietal sulcus, whereas only three children passed these criteria.

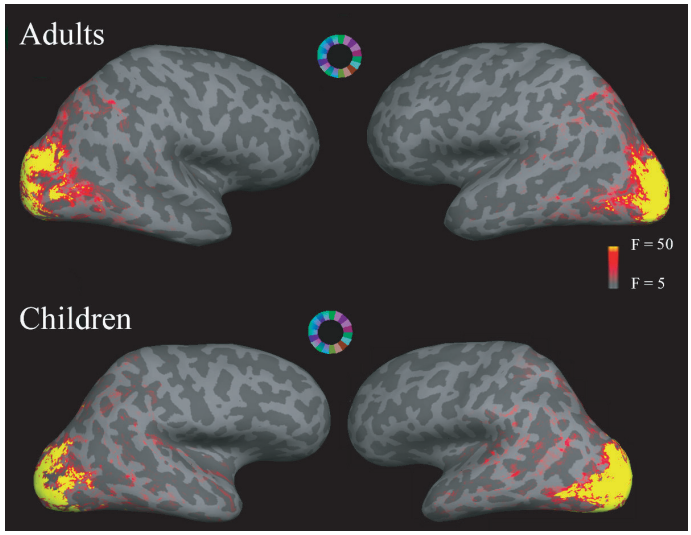

Figure 7. Comparison of eccentricity signals in lateral occipito-temporal cortex for adults and children. Top. The yellow-red color scale shows the Fourier magnitude measured as an *F* statistic averaged across 10 adults and plotted on the lateral view of the inflated right and left hemispheres of one representative adult. The central annular symbol indicates the geometry of the eccentricity stimulus. Bottom. The equivalent data are shown for the group of 10 children. The two groups appear qualitatively similar, except for weak signals observed in the parietal cortex of adults that are not visible for the children.

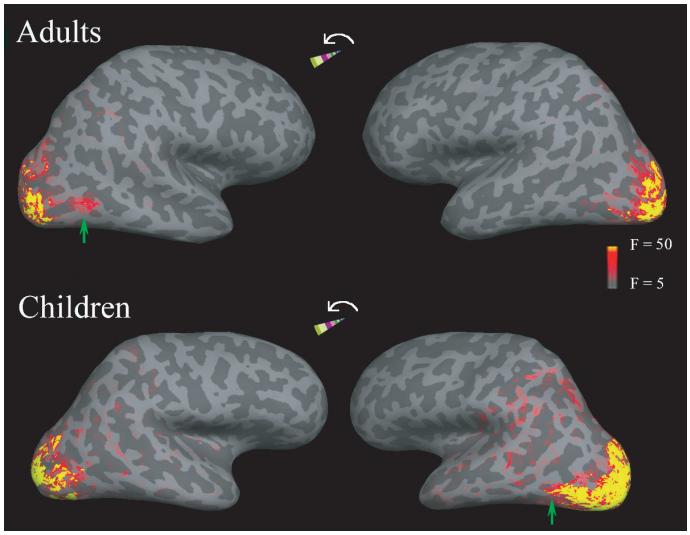

Figure 8. Comparison of polar angle signals in lateral occipito-temporal cortex for adults and children. Top. The yellow-red color scale shows the Fourier magnitude measured as an *F* statistic averaged across 10 adults and plotted on the lateral view of the inflated right and left hemispheres of one representative adult. The central wedge symbol indicates the geometry of the polar angle stimulus. Bottom. The equivalent data are shown for the group of 10 children. The adults and children differ with respect to which hemisphere shows an advantage in the extent of significant signal (highlighted with green arrows).

The results for the polar angle stimulus showed that the children and adults differed in the direction of their hemispheric laterality (Figure 8). The adult group produced more activity in the right hemisphere, whereas the children displayed more activity in the left hemisphere. This finding was consistent at the level of individual subjects. Five adults and six children showed asymmetric activation in the direction stated above, with only one child and adult showing the opposite. This one adult was left-handed, but the child was right-handed.

In contrast to these differences, the maps of Fourier magnitude *F* statistic in adults and children appeared qualitatively similar in the ventral temporal cortices of both hemispheres (Figure 9).

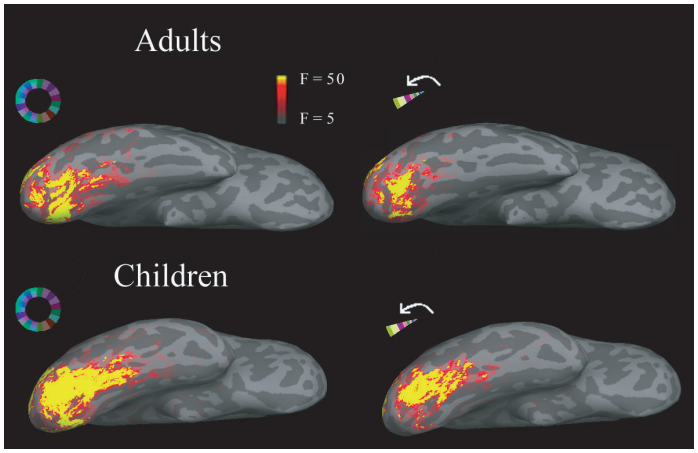

Figure 9. Comparison of eccentricity and of polar angle signals in ventral temporal cortex for adults and children. Top. The yellow-red color scale shows the Fourier magnitude measured as an *F* statistic averaged across 10 adults and plotted on the ventral view of the inflated right hemisphere of one representative adult. The annular or wedge symbols indicate when eccentricity or polar angle data are shown. Bottom. The equivalent data are shown for the group of 10 children. The two groups appear qualitatively similar.

4. Discussion

The results of this study provide a quantitative comparison of retinotopic mapping in adults and children. Retinotopic organization in children older than 9 years and in adults is qualitatively similar, and six classically reported visual areas could be readily identified (V1, V2, V3, V3A, VP, and V4v). Small differences in regional signal magnitude and areal size were documented, and suggest some developmental trends. According to our experience, children younger than 9 years may require more training due

to greater head motion and less attention to task. Extra training may improve success rates for this group.

Although motion artifact appeared to be the major determinant of poor fMRI maps in our youngest subjects (aged 7 and 8 years), we cannot completely exclude immaturity at the neural or hemodynamic levels. The basic mechanism of image contrast in fMRI is known (called blood oxygenation level dependent [BOLD]), but a detailed understanding of the coupling between changes in neural activity and changes in blood oxygenation and flow has not yet been achieved. It is not known if this mechanism changes during the course of development. Some results have indicated a *negative* BOLD response in the visual cortex of sedated infants, raising the possibility of drastic developmental changes in the BOLD mechanism (Born, Rostrup, Leth, Peitersen, & Lou, 1996, 1998; Yamada, Sadato, & Konishi, 1997). Possible reasons for differences in the BOLD signal in children include higher metabolic rates at rest than in adults, perhaps supporting higher synaptic density (e.g., Chugani et al., 1988). However, sedation or sleep may instead be the important variable here. Recently, a negative BOLD response was obtained in children and in adults during slow wave sleep, as well as in some cases of sedated adults (Born et al., 2002). Regardless of the precise role of these factors in infants and young children, our own results and those of others suggest that a positive BOLD response dominates in awake children by age 7-8 (Martin et al., 1999).

There are several other concerns that apply to the comparison of children and adults with fMRI, particularly comparison of magnitude measures. Many equipment-related factors affect the exact magnitude of fMRI signals. Furthermore, unlike PET, fMRI does not provide absolute measures of flow or oxygenation; only relative changes can be detected. FMRI signal can be interpreted only with respect to other "baseline" conditions, which is readily accomplished for within-group comparisons (but see Friston et al., 1996). However, a comparison between groups relies on the assumption that both the baseline and the experimental brain states are the same (e.g., Bookheimer, 2000).

When subjects perform a task during a scan, controlling for task difficulty becomes a concern. If our groups did not perform the same task during the scanning, then it naturally follows that differences in brain activation could be independent of developmental state. In our case, it is possible that the children differed in fixation stability or extrafoveal spatial attention. However, our fixation task did not involve cognitively difficult reasoning or speeded reactions. To reduce the demands on children with regard to sustained vigilance/attention, we administered the scans in units of 4 min rather than 8 min. The adult-like retinotopic maps we obtained from the children suggest that they did indeed maintain fixation and attention. Moreover, for the six retinotopic areas, the main effect was the normalized size of several extrastriate areas, and this selective topographic effect is unlikely to be due solely to one of these confounds.

Minimal differences in signal magnitude between children and adults were observed in the ROI analysis, so we can probably exclude major group differences due to head position in the coil or head motion. Once we excluded the subjects with gross head motion artifacts, we observed no correlation between head motion and Fourier magnitude. We did, however, find that the Fourier magnitude measure was variable in children.

To compare the organization of primary visual cortex in more detail, we computed the cortical magnification function in both children and adults. We found that the children's data did not differ from the adult's for V1 or V2. Our values were highly consistent with those reported by previous studies (Engel et al., 1997). For example, the exponent fitted to the V1 data of Engel et al. was 0.063 for two adults, and the data from Sereno et al. is approximately 0.082. These values are close to our value of 0.074 for 10 adults. Interestingly, the V1 cortical magnification factor has been shown to be correlated with behavioral performance on Vernier acuity tasks (e.g., Duncan & Boynton, 2003). Given that Vernier acuity does not reach adult levels until age 14, the adult-like cortical magnification factor we found for the child group is notable. This may be another example in which development of complex sensorimotor behaviors may lag relative to isolated physiological indices (in visual cortex).

We measured the surface area of retinotopic visual areas in terms of absolute and proportional size. Similar data have recently been reported for absolute size for three visual areas in adults only (Dougherty et al., 2003). These authors obtained mean sizes of 1470, 1115, and 819 mm for V1, V2, and V3. The value for V2 is the same as our measurements, although our estimates for V1 and V3 are lower. There are several methodological differences that could provide an explanation: cortical flattening techniques, our use of field sign computations, and our use of manual versus automatic tracing of visual boundaries. Nonetheless, all of our methods were applied consistently to the adults and children, and should allow meaningful comparison between the two groups.

Our data indicate that extrastriate cortex was measurably smaller in children compared to adults. This result was obtained for both absolute size and percentage of the entire reconstructed neocortical sheet, suggesting that gross brain size is not a relevant factor. Consistently, previous literature indicates no significant change in cerebral volume after age 5 (Giedd et al., 1996; Reiss, Abrams, Singer, Ross, & Denckla, 1996). The idea that extrastriate cortex could mature later than striate cortex is confirmed by the results of some previous reports. Ossenblok et al. (1994) concluded that striate activity dominates the checkerboard onset evoked potential of the children aged about 4–8 years, whereas extrastriate activity grows later in life. A posterior-to-anterior maturation gradient is also suggested by the few available anatomical studies of children's brains (Garey & de Courten, 1983; Thompson et al., 2000; Sowell et al., 1999). Nonetheless, the fact that our data showed adult-like

cortical magnification functions in V2 despite its smaller size in children may indicate that the overall size difference has limited functional significance. Future studies of extrastriate cortical areas in children may help clarify these issues.

We performed whole brain across-subject averaging to assess the regional extent of retinotopic activity in higher level cortex of the parietal, lateral occipital, and temporal cortex. Based on gross anatomical homologies, the eccentricity stimulus results suggest a slight trend toward greater activity in parietal lobes of the adults. However, we cannot easily separate fixation task-related activity from a true difference in retinotopy. Further study of spatial perception and attention in children would be warranted. The most striking difference between children and adults was seen for the polar angle stimulus (Figure 8). However, caution is required when interpreting these data, given that we could not directly compare the hemispheres of adults and children. However, we can still see that within the adult group, the right hemisphere produced more activity, whereas in the child group, the opposite bias was seen. Furthermore, these suggestive differences occur in the absence of differences elsewhere (e.g., ventral temporal cortex).

There is only a small literature that speaks to hemispheric lateralization during human cortical development, but there is evidence that developmental rates do differ between hemispheres. However, no simple left-right gradient is likely to exist, rather, regionally specific effects have often been found at different ages (Thatcher, Walker, & Giudice, 1987; Sowell, Thompson, Tessner, & Toga, 2001). Given our lateralized findings with the moving polar angle stimulus, one study that measured cortical activity during a form-from-motion task in the left or right hemifield is quite relevant (Hollants-Gilhuijs, Ruijter, & Spekreijse, 1998). This cross-sectional ERP study of children and adults concluded that "maturation of motion sensitive areas of the extrastriate cortex in children's right hemisphere is delayed with respect to that of the homologous regions of the left hemisphere." The convergence of their conclusion with our own is suggestive, although clearly more studies that measure visual performance along with brain activity are required. Finally, it may be relevant that cognitive tasks such as analysis of global versus local object structure, when measured with fMRI, do not produce the adult-like degree of hemispheric lateralization in many children aged 12-14 years (Moses et al., 2002).

Despite the subtle differences between adults and children we documented here, the overall similarity between the groups is evident. The rather mature visual maps seen in children aged between 9 and 12 years contrast with many cognitive functions that mature much later, and fMRI is increasingly being employed to study such protracted neurological development. For example, the first pediatric fMRI study focused on immature frontal lobe function as assessed by working memory (Casey et al., 1995). Recent cross-sectional studies of reading (Turkeltaub et al., 2003) and visuo-spatial working memory (Kwon et al., 2002) have included extensive behavioral measures and document impressive amounts of both age- and performance-related change. The relatively stable retinotopic visual representations during the childhood-adolescence period may serve as a baseline for comparison to the more protracted development of anterior regions.

5. Conclusion

In this study, we measured retinotopic organization in children in multiple visual areas for the first time. We demonstrated the feasibility of applying techniques developed for adults, with only slight modifications. The children were not given separate training sessions, although the reports of other investigators indicate that this is an effective strategy and could improve the success rate even further. In the future, the fMRI technique, especially with longitudinal designs, should contribute greatly to studies of brain development because experiments can be repeated to document change over time. Cortical flattening methods can further facilitate the accumulation of data from multiple experiments onto individual maps of visual cortex. It will be possible to compare retinotopic maps in normal children to children with visual disorders and monitor the effect of treatment variables over time, an approach that is already revealing neurological effects of remediation in children with dyslexia (Temple et al., 2003).

Acknowledgments

Supported by COBRE Grant P20RR15574, Project 2, from NIH/NCRR to JM. We thank Mathis Frick, Doug Greve, Bruce Fischl, Sean Marrett, Ray Raylman, and Ruth Walsh for their valuable contributions. Portions of this work were presented at the 2002 Vision Sciences Society Conference in Sarasota, FL (Conner, Sharma & Mendola, 2002).

Commercial Relationships: None.
Corresponding author: Janine Mendola.
Email: jmendola@hsc.wvu.edu.
Address: WVU Health Sciences Center, PO Box 9236, Morgantown, WV 26506, USA.

References

Bookheimer, S. Y. (2000). Methodological issues in pediatric neuroimaging. *Mental Retardation and Developmental Disabilities Research Reviews, 6*(3), 161-165. [PubMed]

Born, A. P., Law, I., Lund, T. E., Rostrup, E., Hanson, L. G., Wildschiodtz, G., et al. (2002). Cortical deactivation induced by visual stimulation in human slow-wave sleep. *Neuroimage, 17*(3), 1325-1335. [PubMed]

Born, P., Leth, H., Miranda, M. J., Rostrup, E., Stensgaard, A., Peitersen, B., et al. (1998). Visual activation in infants and young children studied by functional magnetic resonance imaging. *Pediatric Research, 44*(4), 578-583. [PubMed]

Born, P., Rostrup, E., Leth, H., Peitersen, B., & Lou, H. C. (1996). Change of visually induced cortical activation patterns during development. *Lancet, 347*, 543. [PubMed]

Casey, B. J., Cohen, J. D., Jezzard P., Turner R., Noll, D. C., Trainor, R. J., et al. (1995). Activation of prefrontal cortex in children during a nonspatial working memory task with functional MRI. *Neuroimage, 2*, 221-229. [PubMed]

Chugani, H. T., Shewmon, D. A., Peacock, W. J., Shields, W. D., Mazziotta, J. C., & Phelps, M. E. (1988). Surgical treatment of intractable neonatal-onset seizures: The role of positron emission tomography. *Neurology 38*(8), 1178-1788. [PubMed]

Cox, R. W., & Jesmanowicz, A. (1999). Real-time 3D image registration for functional MRI. *Magnetic Resonance in Medicine, 42*, 1014-1018. [PubMed]

Conner, I. P., Sharma, S., & Mendola, J. D. (2002). Retinotopic mapping in children with normal vision [Abstract]. *Journal of Vision*, *2*(7), 109a, http://journalofvision.org/2/7/109/, doi:10.1167/2.7.109.

Dale, A. M., Fischl, B., & Sereno, M. I. (1999). Cortical surface-based analysis. I. Segmentation and surface reconstruction. *Neuroimage, 9*, 179-194. [PubMed]

DeYoe, E. A., Carman, G. J., Bandettini, P., Glickman, S., Wieser, J., Cox, R., Miller, D., & Neitz, J. (1996). Mapping striate and extrastriate visual areas in human cerebral cortex. *Proceedings of the National Academy of Sciences of the U.S.A., 93*, 2382-2386. [PubMed]

Dougherty, R. F., Koch, V. M., Brewer, A. A., Fischer, B., Modersitzki, J., & Wandell, B. A. (2003). Visual field representations and locations of visual areas V1/V2/V3 in human visual cortex. *Journal of Vision, 3*(10), 586-598, http://journalofvision.org/3/10/1/, doi:10.1167/3.10.1. [PubMed] [Article]

Duncan, R. O., & Boynton, G. M. (2003). Cortical magnification within human primary visual cortex correlates with acuity thresholds. *Neuron, 38*(4), 659-671. [PubMed]

Ellemberg, D., Lewis, T., Liu, C., & Maurer, D. (1999). Development of spatial and temporal vision during childhood. *Vision Research, 39*, 2325-2333. [PubMed]

Engel, S. A., Glover, G. H., & Wandell, B. A. (1997). Retinotopic organization in human visual cortex and the spatial precision of functional MRI. *Cerebral Cortex, 7*, 181-192. [PubMed]

Engel, S. A., Rumelhart, D. E., Wandell, B. A., Lee, A. T., Glover, G. H., Chichilnisky, E. J., & Shadlen, M. N. (1994). fMRI of human visual cortex. *Nature, 369*(6481), 525. [PubMed]

Evans, C., Collins, D. L., Mills, S. R., Brown, E. D., Kelly, R. L., & Peters, T. M. (1993). 3D statistical neuroanatomical models from 305 MRI volumes. *Proceedings IEEE-Nuclear Science Symposium and Medical Imaging Conference*, 1813-1817.

Fischl, B., Sereno, M. I., & Dale, A. M. (1999a). Cortical surface-based analysis. II: Inflation, flattening, and a surface-based coordinate system. *Neuroimage, 9*, 195-207. [PubMed]

Fischl, B., Sereno, M. I., Tootell, R. B., & Dale, A. M. (1999b). High-resolution intersubject averaging and a coordinate system for the cortical surface. *Human Brain Mapping, 8*(4), 272-284. [PubMed]

Fischl, B., & Dale, A. M. (2000). Measuring the thickness of the human cerebral cortex from magnetic resonance images. *Proceedings of the National Academy of Sciences of the U. S. A., 97*(20), 11050-11055. [Pubmed]

Fischl, B., Liu, A., & Dale, A. M. (2001). Automated manifold surgery: Constructing geometrically accurate and topologically correct models of the human cerebral cortex. *IEEE Transactions on Medical Imaging, 20*(1), 70-80. [PubMed]

Friston, K. J., Price, C. J., Fletcher, P., Moore, C., Frackowiak, R. S., & Dolan. R. J. (1996). The trouble with cognitive subtraction. *Neuroimage, 4*(2), 97-104. [PubMed]

Garey, L. J., & de Courten, C. (1983). Structural development of the lateral geniculate nucleus and visual cortex in monkey and man. *Behavioral Brain Research, 10*(1), 3-13. [PubMed]

Giedd, J. N., Snell, J. W., Lange, N., Rajapakse, J. C., Casey, B. J., Kozuch, P. L., et al. (1996). Quantitative magnetic resonance imaging of human brain development: Ages 4-18. *Cerebral Cortex, 6*(4), 551-560. [PubMed]

Glover, G. H. (1999). Simple analytic spiral K-space algorithm. *Magnetic Resonance in Medicine, 42(2)*, 412-415. [PubMed]

Hadjikhani, N., Liu, A. K., Dale, A. M., Cavanagh, P., & Tootell, R. B. (1998). Retinotopy and color sensitivity in human visual cortical area V8. *Nature Neuroscience, 1*(3), 235-241. [PubMed]

Hasson, U., Levy, I., Behrmann, M., Hendler, T., & Malach, R. (2002). Eccentricity bias as an organizing principle for human high-order object areas. *Neuron, 34*, 479-490. [PubMed]

Hollants-Gilhuijs, M. A., Ruijter, J. M., & Spekreijse, H. (1998). Visual half-field development in children: Detection of motion-defined forms. *Vision Research, 38*(5), 651-657. [PubMed]

Kiorpes, L., & Movshon, J. A. (2003). Neural limitations on visual development in primates. In L. Chalupa & J. S. Werner (Eds.), *The visual neurosciences*. Cambridge, MA: MIT Press.

Kovacs, I., Kozma, P., Feher, A., & Benedek, G. (1999). Late maturation of visual spatial integration in humans. *Proceedings of the National Academy of Sciences of the U. S. A., 96*(21), 12204-12209. [PubMed]

Kovacs, I. (2000). Human development of perceptual organization. *Vision Research, 40*(10-12), 1301-1310. [PubMed]

Kwon, H., Reiss, A. L., & Menon, V. (2002). Neural basis of protracted developmental changes in visuo-spatial working memory. *Proceedings of the National Academy of Sciences of the U. S. A., 99*(20), 13336-13341. [PubMed]

Kwong, K., Belliveau, J., Chesler, D., Goldberg, I., Weisskoff, R., Poncelet, B., et al. (1992). Dynamic magnetic resonance imaging of human brain activity. *Proceedings of the National Academy of Sciences of the U. S. A., 89*, 5675-5979. [PubMed]

Logothetis, N. K., Pauls, J., Augath, M., Trinath, T., & Oeltermann, A. (2001). Neurophysiological investigation of the basis of the fMRI signal. *Nature, 412*, 150-157. [PubMed]

Malach, R., Levy, I., & Hasson, U. (2002). The topography of high-order human object areas. *Trends in Cognitive Science, 6*(4), 176-184. [PubMed]

Martin, E., Joeri, P., Loenneker, T., Ekatodramis, D., Vitacco, D., Hennig, J., & Marcar, V. L. (1999). Visual processing in infants and children studied using functional MRI. *Pediatric Research, 46*(2), 135-140. [PubMed]

Mendola, J. D., Dale, A. M., Fischl, B., Liu, A., & Tootell, R. B. H. (1999). The representation of illusory and real contours in human cortical visual areas revealed by fMRI. *Journal of Neuroscience, 19*, 8560-8572. [PubMed]

Moses, P., Roe, K., Buxton, R. B., Wong, E. C., Frank, L. R., & Stiles, J. (2002). Functional MRI of global and local processing in children. *NeuroImage, 16*, 415-424. [PubMed]

Ogawa, S., Tank, D. W., Menon, R., Ellermann, J. M., Kim, S. G., Merkle, H., & Ugurbil, K. (1992). Intrinsic signal changes accompanying sensory stimulation: functional brain mapping with magnetic resonance imaging. *Proceedings of the National Academy of Sciences of the U. S. A., 89*, 5951-5955. [PubMed]

Ossenblok, P., De Munck, J. C., Wieringa, H. J., Reits, D., & Spekreijse, H. (1994). Hemispheric asymmetry in the maturation of the extrastriate checkerboard onset evoked potential. *Vision Research, 34*(5), 581-590. [PubMed]

Regan, D., & Spekreijse, H. (1986). Evoked potentials in vision research 1961-86. *Vision Research, 26*(9), 1461-1480. [PubMed]

Reiss, A. L., Abrams, M. T., Singer, H. S., Ross, J. L., & Denckla, M. B. (1996). Brain development, gender and IQ in children: A volumetric imaging study. *Brain, 119* (Pt 5), 1763-1774. [PubMed]

Rosas, H. D., Liu, A. K., Hersch, S., Glessner, M., Ferrante, R. J., Salat, D. H., et al. (2002). Regional and progressive thinning of the cortical ribbon in Huntington's disease. *Neurology, 58*(5), 695-701. [PubMed]

Sereno, M. I., Dale, A. M., Reppas, J. B., Kwong, K. K., Belliveau, J. W., Brady, T. J., et al. (1995). Borders of multiple visual areas in humans revealed by functional magnetic resonance. *Science, 268*, 889-893. [PubMed]

Sireteanu, R. (2000). Texture segmentation, "pop-out," and feature binding in infants and children. In C. Rovee-Collier, L. Lipsitt, & H. Hayne (Eds.), *Progress in infancy research*, Vol. 1 (pp. 183-250). Mahwah, NJ: Lawrence Erlbaum.

Skoczenski, A. M., & Norcia, A. M. (2002). Late maturation of visual hyperacuity. *Psychological Science, 13*(6), 537-541. [PubMed]

Sowell, E. R., Thompson, P. M., Holmes, C. J., Batth, R., Jernigan, T. L., & Toga, A. W. (1999). Localizing age-related changes in brain structure between childhood and adolescence using statistical parametric mapping. *Neuroimage, 9(6, Pt 1)*, 587-597. [PubMed]

Sowell, E. R., Thompson, P. M., Tessner, K. D., & Toga, A. W. (2001). Mapping continued brain growth and gray matter density reduction in dorsal frontal cortex: Inverse relationships during postadolescent brain maturation. *Journal of Neuroscience, 21*(22), 8819-8829. [PubMed]

Talairach, J., & Tournoux, P. (1988). *Co-planar stereotaxic atlas of the human brain*. New York: Thieme Medical Publishers.

Temple, E., Deutsch, G. K., Poldrack, R. A., Miller, S. L., Tallal, P., Merzenich, M. M., & Gabrieli, J. D. (2003). Neural deficits in children with dyslexia ameliorated by behavioral remediation: Evidence from functional MRI. *Proceedings of the National Academy of Science of the U. S. A., 100*(5), *2860-2865*. [PubMed]

Thatcher, R. W., Walker, R. A., & Giudice, S. (1987). Human cerebral hemispheres develop at different rates and ages. *Science, 236*(4805), 1110-1113. [PubMed]

Thompson, P. M., Giedd, J. N., Woods, R. P., MacDonald, D., Evans, A. C., & Toga, A. W. (2000). Growth patterns in the developing brain detected by using continuum mechanical tensor maps. *Nature, 404*(6774), 190-193. [PubMed]

Tootell, R. B., Hadjikhani, N., Hall, E. K., Marrett, S., Vanduffel, W., Vaughan, J. T., & Dale, A. M. (1998a). The retinotopy of visual spatial attention. *Neuron, 21*(6), 1409-1422. [PubMed]

Tootell, R. B, Mendola, J. D., Hadjikhani, N. K., Liu, A. K., & Dale, A. M. (1998b). The representation of the ipsilateral visual field in human cerebral cortex. *Proceedings of the National Academy of Sciences of the U. S. A., 95*(3), 818-824. [PubMed]

Tootell, R. B. H., Mendola, J. D., Hadjikhani, N. K., Ledden, P. J., Liu, A. K., Reppas, J. B., et al. (1997). Functional analysis of V3A and related areas in human visual cortex. *Journal of Neuroscience, 17*, 7060-7078. [PubMed]

Turkeltaub, P. E., Gareau, L., Flowers, D. L., Zeffiro, T. A., & Eden, G. F. (2003). Development of neural mechanisms for reading. *Nature Neuroscience, 6*(7), 767-773. [PubMed]

Tyschen, L . (1992). Binocular vision. In W. M. Hart (Ed.), *Adler's physiology of the eye: Clinical application (9th ed.)* (pp. 773-852). St. Louis, MI: Mosby.

Wade, A. R., Brewer, A. A., Rieger, J. W., & Wandell, B. A. (2002). Functional measurements of human ventral occipital cortex: Retinotopy and colour. *Philosophical Transactions of the Royal Society of London B, 357*(1424), 963-973. [PubMed]

Yamada, H., Sadato, N., & Konishi, Y. (1997). A rapid brain metabolic change in infants detected by fMRI. *Neuroreport, 8*, 3775-3778. [PubMed]